Editors' Suggestion

Stochastic ferrimagnetic Landau-Lifshitz-Bloch equation for finite magnetic structures

Christoph Vogler,* Claas Abert, Florian Bruckner, and Dieter Suess
Christian Doppler Laboratory for Advanced Magnetic Sensing and Materials, Faculty of Physics, University of Vienna, Boltzmanngasse 5, 1090 Vienna, Austria

(Received 17 January 2019; revised manuscript received 31 May 2019; published 1 August 2019)

Precise modeling of the magnetization dynamics of nanoparticles with finite-size effects at fast varying temperatures is a computationally challenging task. Based on the Landau-Lifshitz-Bloch (LLB) equation we derive a coarse-grained model for disordered ferrimagnets, which is both fast and accurate. First, we incorporate stochastic fluctuations to the existing ferrimagnetic LLB equation. Further, we derive a thermodynamic expression for the temperature-dependent susceptibilities, which is essential to model finite-size effects. Together with the zero-field equilibrium magnetization the susceptibilities are used in the stochastic ferrimagnetic LLB to simulate a ferrimagnetic $Gd_{30}(FeCo)_{70}$ particle with a diameter of 5 nm and a height of 10 nm under various external applied fields and heat pulses. The obtained trajectories agree well with those of an atomistic model, which solves the stochastic Landau-Lifshitz-Gilbert equation for each atom. Finally, we apply a 50-fs heat pulse with a maximum temperature of 1193 K to a $Gd_{24}(FeCo)_{76}$ particle of the same size to test the proposed model for all-optical switching (AOS). We observe switching with a ferromagneticlike state, which was identified to be the key for AOS in GdFeCo. Although the coarse-grained model in general shows remarkably good agreement with atomistic simulations, the computed switching probability is lower than expected. The magnetization trajectories seem to be too far away from equilibrium for ultrashort and very high heat pulses, which are typical for AOS. This leads to the conclusion that either the model needs higher-order corrections to accurately describe AOS, or that the two-spin model is not capable of describing deterministic AOS at all.

DOI: 10.1103/PhysRevB.100.054401

I. INTRODUCTION

The calculation of the magnetization dynamics of large systems under the influence of fast varying temperatures is of great interest from both the scientific and the technological perspectives. Heat-assisted magnetic recording (HAMR) [1–5] should be mentioned first and foremost here. Despite the computing power of modern supercomputers, coarse-grained models are needed to manage the computational effort created by such complex systems. The development of the Landau-Lifshitz-Bloch (LLB) equation for pure ferromagnets by Garanin [6] and the subsequent improvements [7–9] paved the way to make concrete design proposals for real HAMR devices [10–14].

Recently it was discovered that the magnetization of disordered ferrimagnetic materials can be reversed by the mere exposure of circularly polarized femtosecond laser pulses [15]. This effect, which was observed in GdFeCo, was called all-optical helicity-dependent switching (AO-HDS). The underlying origin was the basis of many discussions and has still not been fully clarified [16–22]. In addition, it was discovered that the applied laser pulses do not necessarily have to be circularly polarized to reverse the magnetization in GdFeCo and that there exists also a purely thermally induced magnetization switching (TIMS) [23]. All-optical switching has also been detected in other ferrimagnets like TbFe [21,24], TbCo [25–28], TbFeCo [29], artificial zero-moment magnets [30], and even in multilayer structures without any rare-earth atoms [27,31]. All these observations give hope that AO-HDS or TIMS could be used in magnetic recording devices.

In recent years, ferrimagnetic materials have also found their way into spintronics. Due to the fast magnetization dynamics in antiferromagnetically coupled systems and their insensitivity to external fields near the compensation point, ferrimagnetic materials are an ideal candidate for spin-orbit torque magnetoresistive random access memory (SOT-MRAM) [32–38]. But also concepts like thermally assisted spin-transfer torque MRAM (STT-MRAM), in which Joule heating of the current through the cell is used to switch the GdFeCo/TbFe free layer [39], show the great technological relevance of ferrimagnetic materials.

As a consequence an efficient coarse-grained model of disordered ferrimagnets with finite size is essential to investigate the feasibility of magneto-optical recording of ferrimagnetic materials or spintronic devices with ferrimagnetic layers in detail and to develop design guidelines.

Similar to the derivation of the Landau-Lifshitz-Bloch (LLB) equation for pure ferromagnets by Garanin [6], Atxitia *et al.* [40] have recently shown how the LLB equation can be adapted for disordered ferrimagnets with two sublattices. Before going into detail and presenting extensions to ferrimagnetic LLB equation, we would like to briefly review the results of Ref. [40]. The temporal evolution of the reduced magnetization $\boldsymbol{m}_\mathrm{A} = \boldsymbol{M}_\mathrm{A}/M_{\mathrm{A},0}$ (with $M_{\mathrm{A},0}$ being the zero temperature sublattice saturation magnetization) of

*christoph.vogler@univie.ac.at

sublattice A can be calculated per

$$\frac{\partial \boldsymbol{m}_\mathrm{A}}{\partial t} = -\mu_0\gamma'_\mathrm{A}(\boldsymbol{m}_\mathrm{A}\times\boldsymbol{H}_\mathrm{eff,A}) + \frac{\mu_0\gamma'_\mathrm{A}\alpha^\parallel_\mathrm{A}}{m^2_\mathrm{A}}(\boldsymbol{m}_\mathrm{A}\cdot\boldsymbol{H}_\mathrm{eff,A})\boldsymbol{m}_\mathrm{A} - \frac{\mu_0\gamma'_\mathrm{A}\alpha^\perp_\mathrm{A}}{m^2_\mathrm{A}}[\boldsymbol{m}_\mathrm{A}\times(\boldsymbol{m}_\mathrm{A}\times\boldsymbol{H}_\mathrm{eff,A})], \tag{1}$$

where γ'_A is the reduced electron gyromagnetic ratio $\gamma'_\mathrm{A} = \gamma_\mathrm{e}/(1+\lambda^2_\mathrm{A})$, which is defined via the coupling parameter λ_A of sublattice A to the heat bath and $\alpha^\perp_\mathrm{A}$ and $\alpha^\parallel_\mathrm{A}$ are the perpendicular and the parallel dimensionless damping constant, respectively. Below T_C they are defined per

$$\alpha^\parallel_\mathrm{A} = 2\lambda_\mathrm{A}k_\mathrm{B}T\frac{m_\mathrm{e,A}}{J_{0,\mathrm{AA}}m_\mathrm{e,A} + |J_{0,\mathrm{AB}}|m_\mathrm{e,B}}, \tag{2}$$

$$\alpha^\perp_\mathrm{A} = \lambda_\mathrm{A}\left(1 - k_\mathrm{B}T\frac{m_\mathrm{e,A}}{J_{0,\mathrm{AA}}m_\mathrm{e,A} + |J_{0,\mathrm{AB}}|m_\mathrm{e,B}}\right), \tag{3}$$

with $m_\mathrm{e,A}$ and $m_\mathrm{e,B}$ being the equilibrium magnetization in sublattices A and B, respectively. In the case of two sublattices with atoms A and B there exist three exchange energies, $J_\mathrm{A\text{-}A}$, $J_\mathrm{B\text{-}B}$, and $J_\mathrm{A\text{-}B}$. The exchange energies in the LLB model depend on the number of nearest neighbors z and on the concentrations x_A of the atoms. Hence, the exchange energies become $J_{0,\mathrm{AA}} = zx_\mathrm{A}J_\mathrm{A\text{-}A}$ and $J_{0,\mathrm{BA}} = zx_\mathrm{A}J_\mathrm{A\text{-}B}$. Above T_C we use the definition of the damping constants according to Ref. [41] per

$$\alpha^\parallel_\mathrm{A} = \alpha^\perp_\mathrm{A} = \frac{2\lambda_\mathrm{A}T}{3T_\mathrm{C}} \tag{4}$$

It is not surprising that Eq. (1) is of the same form as the ferromagnetic LLB equation, because within each sublattice the magnetizations and the field terms are treated with the mean-field approximation usually used for ferromagnets. The effective field $\boldsymbol{H}_\mathrm{eff,A}$ of each sublattice is defined per [40]

$$\boldsymbol{H}_\mathrm{eff,A} = \boldsymbol{H}_\mathrm{ext} + \boldsymbol{H}_\mathrm{ani,A} + \boldsymbol{H}_\mathrm{ex,A} + \boldsymbol{H}^\parallel_\mathrm{eff,A} \tag{5}$$

with

$$\mu_0\boldsymbol{H}_\mathrm{ani,A} = \frac{2d_\mathrm{A}}{\mu_\mathrm{A}}m_{z,\mathrm{A}}\boldsymbol{e}_z, \tag{6}$$

$$\mu_0\boldsymbol{H}_\mathrm{ex,A} = -\frac{J_{0,\mathrm{AB}}}{\mu_\mathrm{A}m^2_\mathrm{A}}[\boldsymbol{m}_\mathrm{A}\times(\boldsymbol{m}_\mathrm{A}\times\boldsymbol{m}_\mathrm{B})], \tag{7}$$

$$\mu_0\boldsymbol{H}^\parallel_\mathrm{eff,A} = -\left(\frac{1}{\tilde{\chi}^\parallel_\mathrm{A}} + \frac{|J_{0,\mathrm{AB}}|}{\mu_\mathrm{A}}\frac{\tilde{\chi}^\parallel_\mathrm{B}}{\tilde{\chi}^\parallel_\mathrm{A}}\right)\frac{\delta m_\mathrm{A}}{m_\mathrm{e,A}}\boldsymbol{m}_\mathrm{A} + \frac{|J_{0,\mathrm{AB}}|}{\mu_\mathrm{A}}\frac{\delta\tau_\mathrm{B}}{m_\mathrm{e,A}}\boldsymbol{m}_\mathrm{A}, \tag{8}$$

and

$$\tau_\mathrm{B} = \frac{|\boldsymbol{m}_\mathrm{A}\cdot\boldsymbol{m}_\mathrm{B}|}{m_\mathrm{A}}. \tag{9}$$

Here, μ_A is the magnetic moment of each spin in sublattice A, d_A is the uniaxial anisotropy energy per spin, and $\tilde{\chi}^\parallel_\mathrm{A}$ is the longitudinal susceptibility of the sublattice. In sublattice B the same quantities are defined. In contrast to Ref. [40] but similar to Ref. [41] we use a linear approximation of $\delta m_\mathrm{A} = m_\mathrm{A} - m_\mathrm{e,A}$ and $\delta\tau_\mathrm{B} = \tau_\mathrm{B} - \tau_\mathrm{e,B}$ in Eq. (8). At the Curie temperature $m_\mathrm{e,A}$ and $\tau_\mathrm{e,B}$ vanish. Under the assumption that the magnetization relaxes fast towards its equilibrium value, $m_\mathrm{e,A}$ can be approximated with m_A to avoid numerical singularities. Hence, Eq. (8) can be extended to temperatures above T_C as follows:

$$\mu_0\boldsymbol{H}^\parallel_\mathrm{eff,A} = -\left(\frac{1}{\tilde{\chi}^\parallel_\mathrm{A}} + \frac{|J_{0,\mathrm{AB}}|}{\mu_\mathrm{A}}\frac{\tilde{\chi}^\parallel_\mathrm{B}}{\tilde{\chi}^\parallel_\mathrm{A}}\right)\boldsymbol{m}_\mathrm{A} + \frac{|J_{0,\mathrm{AB}}|}{\mu_\mathrm{A}}\frac{\tau_\mathrm{B}}{m_\mathrm{A}}\boldsymbol{m}_\mathrm{A} \quad \text{if} \quad T \geqslant T_\mathrm{C}. \tag{10}$$

This field is equivalent to the corresponding expression at high temperatures of Ref. [41]. Note that all equations are identical for sublattice B if subscript A is replaced by subscript B.

The described formalism was successfully applied in the past [22,42–45]. Most of these works investigate fast relaxation processes in ferrimagnets and use a simplified or a linearized version of the ferrimagnetic LLB. Due to the deterministic nature of Eq. (1) all results can be interpreted as ensemble averages. We are interested in the full dynamical response of ferrimagnets with finite size under arbitrary external conditions. In the presence of temperature, this response has a stochastic nature.

II. EXTENSIONS TO THE FERRIMAGNETIC LLB EQUATION

A. Stochastic form

To account for stochastic fluctuations due to temperature we follow the derivations of Evans *et al.* [8] for the LLB equation for ferromagnets, which lead to a Boltzmann distribution of the magnetization in equilibrium. The basic assumption is that thermal fluctuations can be introduced to the LLB via thermal fields. These fields are uncorrelated in time and space, which means that their components consist of white-noise random numbers with zero mean and a variance of

$$\left\langle\xi^\eta_{\kappa,i}(t,\boldsymbol{r})\xi^\eta_{\kappa,j}(t',\boldsymbol{r}')\right\rangle = 2D^\eta_\kappa\delta_{ij}\delta(\boldsymbol{r}-\boldsymbol{r}')\delta(t-t'), \tag{11}$$

where i, j are the Cartesian components of the thermal field, κ is a placeholder for the sublattice type (A or B), and η is a placeholder for parallel and perpendicular field components. The four diffusion constants D^η_κ are to be determined for the specific problem. To achieve this there exist two strategies, one by means of the fluctuation dissipation theorem and one via the Fokker-Planck equation. We use the latter approach, which is presented in detail in Appendix, to make the main part of the article more readable. As shown in Appendix we get the following diffusion constants for sublattice A:

$$D^\perp_\mathrm{A} = \frac{(\alpha^\perp_\mathrm{A} - \alpha^\parallel_\mathrm{A})l^3_\mathrm{at}k_\mathrm{B}T}{(\alpha^\perp_\mathrm{A})^2\gamma'_\mathrm{A}\mu^2_0 n_\mathrm{at}x_\mathrm{A}\mu_\mathrm{A}V}, \tag{12}$$

$$D^\parallel_\mathrm{A} = \frac{\alpha^\parallel_\mathrm{A}\gamma'_\mathrm{A}l^3_\mathrm{at}k_\mathrm{B}T}{n_\mathrm{at}x_\mathrm{A}\mu_\mathrm{A}V}. \tag{13}$$

In these equations V is the discretization volume, l_at is the lattice constant, n_at is the number of atoms per unit cell, T is

the temperature, and k_B is the Boltzmann constant. With the diffusion constants, the corresponding stochastic LLB equation for ferrimagnets can be finally obtained (see Appendix) per

$$\frac{\partial \boldsymbol{m}_A}{\partial t} = -\mu_0\gamma'_A(\boldsymbol{m}_A \times \boldsymbol{H}_{\mathrm{eff,A}}) + \frac{\mu_0\gamma'_A\alpha_A^{\parallel}}{m_A^2}(\boldsymbol{m}_A \cdot \boldsymbol{H}_{\mathrm{eff,A}})\boldsymbol{m}_A + \boldsymbol{\xi}_A^{\parallel} - \frac{\mu_0\gamma'_A\alpha_A^{\perp}}{m_A^2}\{\boldsymbol{m}_A \times [\boldsymbol{m}_A \times (\boldsymbol{H}_{\mathrm{eff,A}} + \boldsymbol{\xi}_A^{\perp})]\}. \tag{14}$$

B. Finite system susceptibilities

To integrate the LLB equation detailed knowledge of the longitudinal susceptibilities $\tilde{\chi}_A^{\parallel}$ and $\tilde{\chi}_B^{\parallel}$ are required. In the original work of Atxitia *et al.* [40] a mean-field approach was derived:

$$\tilde{\chi}_{\mathrm{A,mean}}^{\parallel} = \frac{\mu_B\mathcal{L}'_A(\zeta_A)|J_{0,AB}|\mathcal{L}'_B(\zeta_B) + \mu_A\mathcal{L}'_A(\zeta_A)[k_BT - J_{0,BB}\mathcal{L}'_B(\zeta_B)]}{[k_BT - J_{0,AA}\mathcal{L}'_A(\zeta_A)][k_BT - J_{0,BB}\mathcal{L}'_B(\zeta_B)] - |J_{0,BA}|\mathcal{L}'_A(\zeta_A)|J_{0,AB}|\mathcal{L}'_B(\zeta_B)}. \tag{15}$$

In this equation $\mathcal{L}_A$ is the Langevin function with argument $\zeta_A = (J_{0,AA}m_A + |J_{0,AB}|m_B)/(k_BT)$ and $\mathcal{L}'_A$ is the corresponding derivative with respect to ζ_A. Equation (15) is, strictly speaking, correct only for infinite systems. This discrepancy was already extensively discussed in the case of pure ferromagnets [7,9,46]. Additionally, the importance of modeling the temperature dependence of the anisotropy field was shown. By means of the perpendicular susceptibility the anisotropy field in each sublattice can be defined as

$$\boldsymbol{H}_{\mathrm{ani,A}} = \frac{1}{\tilde{\chi}_A^{\perp}}(m_{x,A}\boldsymbol{e}_x + m_{y,A}\boldsymbol{e}_y). \tag{16}$$

Here, the temperature dependence is included in $\tilde{\chi}_A$.

Spin fluctuations at zero field parallel and perpendicular to the anisotropy axis can be used to derive an expression for the response functions. How this is done for a ferromagnet is briefly reviewed in the following. The result will help to derive the susceptibilities of sublattices in a ferrimagnet. The canonical partition function Z of magnetization $\boldsymbol{M}_i$ in microstate i, which is subject to a field $\boldsymbol{B}$, can be expressed per

$$Z = \sum_i e^{-\beta(E_i - V\boldsymbol{M}_i\cdot\boldsymbol{B})}. \tag{17}$$

The expectation value of the magnetization can be written as

$$\langle \boldsymbol{M}\rangle = \frac{1}{Z}\sum_i \boldsymbol{M}_i e^{-\beta(E_i - V\boldsymbol{M}_i\cdot\boldsymbol{B})} = \frac{1}{Z}\frac{1}{\beta V}\frac{\partial Z}{\partial \boldsymbol{B}}. \tag{18}$$

A similar expression for the expectation value of the squared magnetization can be easily found per

$$\langle \boldsymbol{M}^2\rangle = \frac{1}{Z}\frac{1}{\beta^2V^2}\frac{\partial^2 Z}{\partial \boldsymbol{B}^2}. \tag{19}$$

Based on the definition of the susceptibility

$$\boldsymbol{\chi} = \left(\frac{\partial\langle \boldsymbol{M}\rangle}{\partial \boldsymbol{H}}\right)_T = \mu_0\left(\frac{\partial\langle \boldsymbol{M}\rangle}{\partial \boldsymbol{B}}\right)_T, \tag{20}$$

Eqs. (18) and (19) can be used to calculate χ per

$$\boldsymbol{\chi} = \mu_0\beta V[\langle \boldsymbol{M}^2\rangle - \langle \boldsymbol{M}\rangle^2]. \tag{21}$$

Obviously, the same expressions hold for the components of the susceptibility

$$\chi^{\eta} = \mu_0\beta V\left[\left\langle M_\eta^2\right\rangle - \langle M_\eta\rangle^2\right]. \tag{22}$$

We now assume that the ferromagnet is split into two sublattices with concentrations x_A and x_B, with $x_A + x_B = 1$. Hence, the partition function can be written as

$$Z = \sum_i e^{-\beta[E_i - (x_A + x_B)V\boldsymbol{M}_i\cdot\boldsymbol{B}]}. \tag{23}$$

The same procedure as shown above can now be applied to obtain the susceptibility

$$\chi^{\eta} = \mu_0\beta(x_A + x_B)V\left[\left\langle M_\eta^2\right\rangle - \langle M_\eta\rangle^2\right]. \tag{24}$$

Obviously, χ^{η} can be divided into two expressions for the corresponding sublattices. Without loss of generality we further analyze just the susceptibility of sublattice A in the y direction resulting in

$$\chi_A^y = \chi_A^{\perp} = \mu_0\beta x_A V\left[\left\langle M_y^2\right\rangle - \langle M_y\rangle^2\right] = \frac{\mu_0\beta}{x_A V}[\langle (x_A V M_y)^2\rangle - \langle x_A V M_y\rangle^2]. \tag{25}$$

The expression $x_A V M_y = \sum_i^{N_A} \boldsymbol{e}_y \cdot \boldsymbol{\mu}_i$ can be identified with the total magnetic moment of sublattice A in the y direction resulting in

$$\chi_A^{\perp} = \frac{\mu_0\beta(N_A\mu_A)^2}{x_A V}\left[\left\langle \left(m_A^y\right)^2\right\rangle - \left\langle m_A^y\right\rangle^2\right], \tag{26}$$

with the normalized magnetization of the sublattice

$$m_A^y = \frac{\sum_i^{N_A} \boldsymbol{e}_y \cdot \boldsymbol{\mu}_i}{N_A\mu_A}. \tag{27}$$

The sum is over all N_A atoms in sublattice A. In Eq. (16) we are interested in the quantity $\tilde{\chi}_A^{\perp} = \chi_A^{\perp}/(\mu_0 M_{A,0})$. Hence, the final expression takes the following form:

$$\tilde{\chi}_A^{\perp} = \frac{\beta(N_A\mu_A)^2}{x_A V}\frac{l_{at}^3}{n_{at}x_A\mu_A}\left[\left\langle \left(m_A^y\right)^2\right\rangle - \left\langle m_A^y\right\rangle^2\right] = \frac{N_A\mu_A}{k_BT}\frac{1}{x_A}\left[\left\langle \left(m_A^y\right)^2\right\rangle - \left\langle m_A^y\right\rangle^2\right]. \tag{28}$$

Here, l_{at} is the lattice constant and n_{at} is the number of atoms per unit cell. In contrast to $\tilde{\chi}^{\perp}$ of a single-lattice ferromagnet

TABLE I. Geometry and material parameters of both sublattices A and B in $Gd_{30}(FeCo)_{70}$ (taken from Ref. [40]). d is the anisotropy energy per atom, μ is the magnetic moment in units of Bohr magnetons, x is the concentration, $J_{\kappa\text{-}\kappa}$ denotes the exchange energy per atom link between equal atoms, $J_{\kappa\text{-}\nu}$ denotes the exchange energy per atom link between different atoms, λ is the damping constant, n_{at} is the number of atoms per unit cell, l_{at} is the lattice parameter, and r and h are the radius and the height of the cylindrical particle. Curie temperature and compensation point are denoted with T_{C} and T_{comp}, respectively.

	A (FeCo)	B (Gd)
d (J)	$8.072\,51 \times 10^{-24}$	$8.072\,51 \times 10^{-24}$
μ (μ_{Bohr})	2.217	7.63
x (%)	70	30
$J_{\kappa-\kappa}$ (J)	4.5×10^{-21}	1.26×10^{-21}
$J_{\kappa-\nu}$ (J)	-1.09×10^{-21}	
λ	0.1	0.1
n_{at}	4	
r (nm)	5.0	
h (nm)	10.0	
T_{C} (K)	697	
T_{comp} (K)	313	

a factor x_{A}^{-1} appears in the susceptibility of the ferromagnetic sublattice $\tilde{\chi}_{\text{A}}^{\perp}$. Since for total number of atoms $N = N_{\text{A}}/x_{\text{A}}$ holds, the prefactor in Eq. (28) depends on the total number of atoms rather than the number of atoms of the sublattice. This is an important but nonobvious result.

To better understand the result the magnetization of a cylindrical $Gd_{30}(FeCo)_{70}$ particle is computed with the atomistic code VAMPIRE [47], which solves the stochastic Landau-Lifshitz-Gilbert equation for each spin. Material and geometry parameters of the simulated particle are given in Table I. In detail, at a temperature of 1 K system trajectories with 10^7 time steps (after 2×10^4 equilibration steps) with an integration time step of 10^{-15} s are calculated for various values of the exchange $J_{\text{A-B}}$ between atoms A and B. From each trajectory the variance of the y component of the normalized sublattice magnetizations is extracted and shown in Fig. 1. We see that at full exchange the fluctuations are suppressed. At low exchange the fluctuations increase towards the expected value corresponding to the anisotropy field (dashed lines in Fig. 1). This result is clear because the anisotropy field is independent from the distance between the atoms and for two separated not interacting ferromagnets we must obtain the correct anisotropy field. Note that the normalized magnetization fluctuations are plotted, so it is reasonable that the fluctuations of both sublattices are identical for strong exchange coupling. Hence, the fluctuations must be multiplied by the total number of atoms to obtain the correct sublattice susceptibilities. One could also argue that at full exchange the number of nearest neighbors of the same atom type is smaller by a factor of x_ν which obviously also reduces the fluctuations by the same amount. Hence, for full exchange a correction factor of $1/x_\nu$ according to Eq. (28) is needed in the sublattice susceptibilities compared to the ferromagnetic case in order to recover the correct anisotropy field of the sublattices from spin fluctuations.

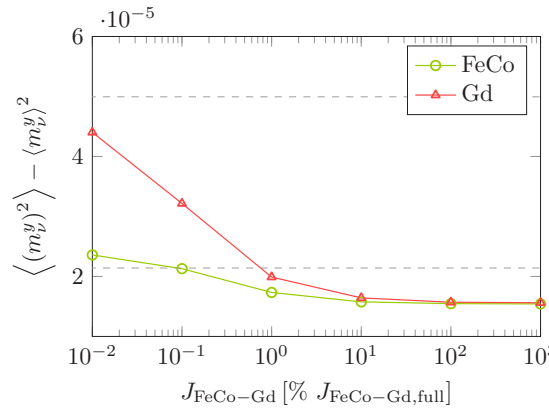

FIG. 1. Variance of the y component of the normalized sublattice magnetizations of $Gd_{30}(FeCo)_{70}$ (parameters are given in Table I) for various values of the exchange $J_{\text{FeCo-Gd}}$ between FeCo atoms and Gd atoms. The horizontal dashed lines represent the expected variances based on the anisotropy fields of the materials.

C. Preparation of material functions

To compute the required temperature-dependent material functions (equilibrium magnetizations and susceptibilities) for the ferrimagnetic LLB equation the atomistic code VAMPIRE [47] is used. Again, system trajectories with 10^7 time steps (after 2×10^4 equilibration steps) with an integration time step of 10^{-15} s are simulated for various temperatures. From these trajectories the zero-field equilibrium magnetizations of the sublattices of the ferrimagnet as well as the susceptibilities via Eq. (28) can be extracted. Note that the magnetization dynamics of such an atomistic reference model are assumed to be correct in a sense that we aim to reproduce them with the presented coarse-grained ferrimagnetic LLB model. Nevertheless, the atomistic data cannot be directly used as input for the LLB equation, because the latter requires temperature-dependent functions of an infinite system. Hence, functions from a mean-field model are typically fitted to the atomistic data. To show how this procedure works for ferrimagnets we would like to rely on an example. For better comparability with Ref. [40] we use a cylindrical nanoparticle consisting of $Gd_{30}(FeCo)_{70}$ as the sample system. The geometry and the material parameters of the particle are shown in Table I. System trajectories at temperatures in the range of 0–950 K are simulated. Figure 2 displays the resulting equilibrium magnetization at zero field for both sublattices. To use these data in Eq. (8) we first fit the FeCo curve $m_{\text{e,A}}$ with the mean-field expression

$$m_{\text{e}}(T) = c_1 \left(1 - \frac{T}{c_2}\right)^{c_3}, \tag{29}$$

with fit parameters c_1, c_2, and c_3. Here, the Curie temperature $T_{\text{C}} = c_2 = 697$ K of the ferrimagnet is determined. In the fit procedure of the second sublattice this Curie temperature is fixed and the remaining two parameters are fitted. The resulting fit functions are plotted in Fig. 2 with black solid lines.

The same trajectories from which the equilibrium magnetizations were determined can also be used to calculate

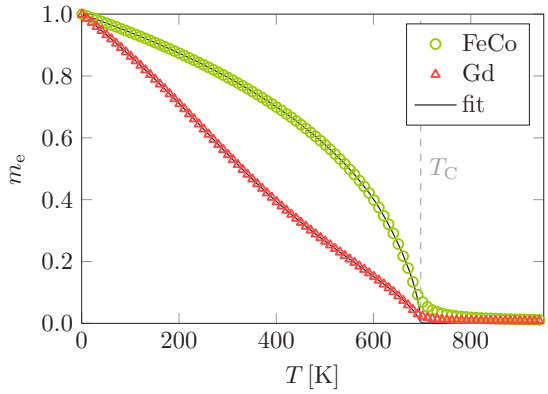

FIG. 2. Zero-field equilibrium magnetization m_e vs temperature, computed with an atomistic model of $Gd_{30}(FeCo)_{70}$ (parameters are given in Table I). The black solid lines show fits, representing an infinite system.

the fluctuations of the magnetization perpendicular to the anisotropy axis by means of Eq. (28). $\tilde{\chi}^{\perp}$ for both sublattices is shown in Fig. 3. The fit of the atomistic data consists of three piecewise continuously differentiable functions per

$$\widetilde{\chi}_{\perp}(T) = \begin{cases} c_4 m_e^{c_5} & T \ll T_C \\ \frac{c_6}{T - T_C} & T > T_C \end{cases}, \tag{30}$$

with c_4–c_6 being fit parameters. In the intermediate temperature range a fourth-order polynomial is used. Since $\widetilde{\chi}_{\perp}(T)$ must be continuously differentiable at the connections only one free parameter remains to fit this polynomial and to close the gap. For further details please refer to Ref. [9]. With the expression [Eq. (28)] derived in Sec. II B the susceptibilities agree well with the inverse anisotropy field at zero temperature, which is also displayed as dashed line in Fig. 3 for both sublattices. At first sight the temperature dependence of the Gd susceptibility seems to be counterintuitive, since it is inversely proportional to the anisotropy field, and thus an increasing anisotropy field could be expected. But, according to Eq. (16) we also must consider the deceasing magnitude of the magnetization. Overall, the anistropy field decreases with

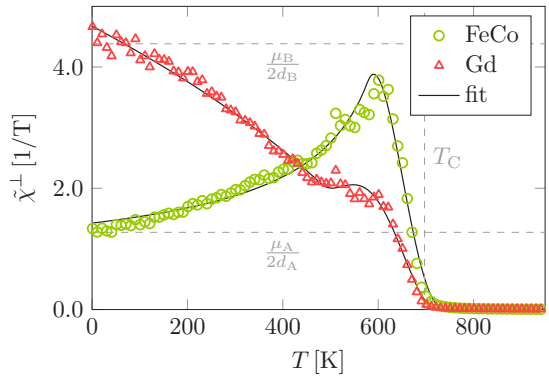

FIG. 3. Perpendicular susceptibility $\tilde{\chi}^{\perp}$, computed with an atomistic model of $Gd_{30}(FeCo)_{70}$ (parameters are given in Table I) from magnetization fluctuations. The black solid lines show fits, representing an infinite system.

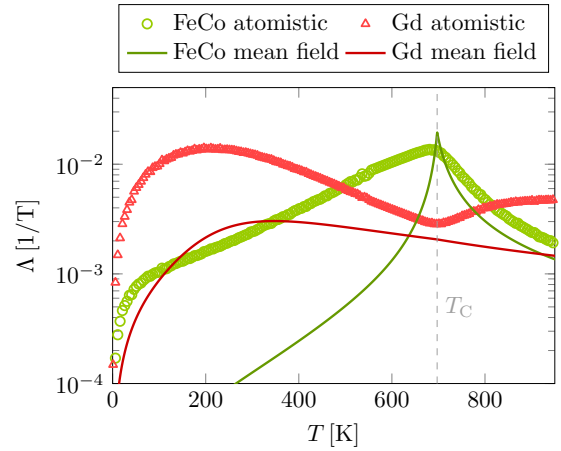

FIG. 4. Temperature evolution of Λ for $Gd_{30}(FeCo)_{70}$ (parameters are given in Table I), based on Eq. (31) with the mean-field expression of Eq. (15) and with the longitudinal susceptibilities obtained by atomistic simulations from fluctuations of the z component of the magnetization.

temperature for both sublattices as expected. Note that the susceptibilities change considerably with temperature. This fact suggests that it is very important to correctly model the temperature dependence of $\tilde{\chi}^{\perp}$ and not only to use the zero-temperature value for the whole temperature range. A detailed comparison will be presented in Sec. III.

Instead of extracting the individual longitudinal susceptibilities from the atomistic data, which is normally done for ferromagnets, we compute the mean-field expression

$$\Lambda_{AA}^{-1} = \left(\frac{1}{\tilde{\chi}_A^{\parallel}} + \frac{|J_{0,AB}|}{\mu_A} \frac{\tilde{\chi}_B^{\parallel}}{\tilde{\chi}_A^{\parallel}} \right) \tag{31}$$

of Eqs. (8) and (10). For the longitudinal susceptibilities Eq. (15) is used. Since the mean-field approach yields a higher Curie point $T_{C,mean} > T_C$ the obtained curves are scaled to fit the finite-size Curie temperature per

$$\Lambda_{AA}(T') = \Lambda_{AA}\left(T \frac{T_C}{T_{C,mean}} \right). \tag{32}$$

For temperatures above T_C the derivative of the Langevin function simplifies to $\mathcal{L}'_A(\zeta_A) = 1/3$. Hence, $\Lambda_{AA}(T)$ is a well defined and continuous function for all temperatures. Figure 4 illustrates $\Lambda_{AA}(T)$ for the used $Gd_{30}(FeCo)_{70}$.

There are two reasons for not using the data of the atomistic simulations for the longitudinal susceptibilities in the computation of Λ. The first reason originates from the fact that the LLB equation requires temperature-dependent functions of an infinite system as input. To get the appropriate $\Lambda(T)$ one could fit the longitudinal susceptibilities analogous to the ferromagnetic LLB equation (see Ref. [9]) and use it in Eq. (31). Since the longitudinal susceptibilities diverge near the Curie point small inaccuracies of the fit functions then lead to fluctuations of $\tilde{\chi}_B^{\parallel}/\tilde{\chi}_A^{\parallel}$, resulting in a wrong system behavior near T_C. Alternatively, atomistic data for $\tilde{\chi}_A^{\parallel}$ and $\tilde{\chi}_B^{\parallel}$ can be directly used to calculate Λ, as shown in Fig. 3. In this case the behavior near T_C is also not correctly reproduced, but we get at least continuous functions

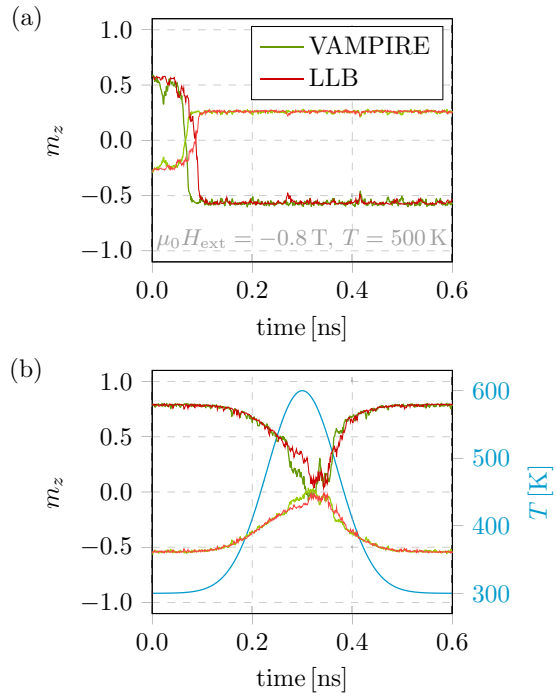

FIG. 5. Temporal evolution of the z component of the normalized magnetization of both sublattices of $Gd_{30}(FeCo)_{70}$ computed with the proposed coarse-grained ferrimagnetic LLB model and the atomistic code VAMPIRE. (a) A constant magnetic field with $\mu_0 H_{\text{ext}} = -0.8$ T and an angle of 6° with the z direction is applied. (b) A Gaussian shaped heat pulse is applied (blue solid line, right y axis).

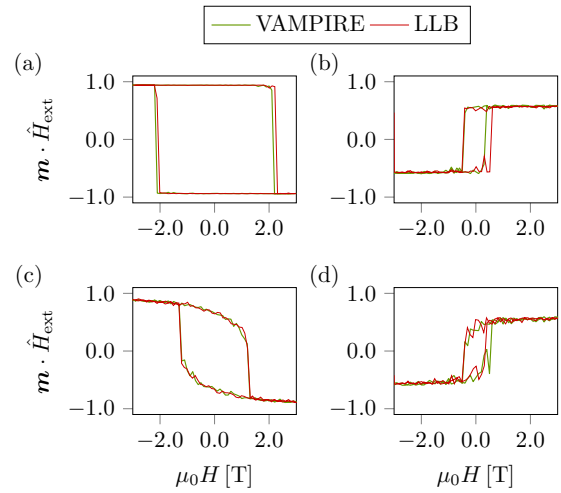

FIG. 6. Hysteresis loops of $Gd_{30}(FeCo)_{70}$ with a field rate of 1 T/ns calculated with the proposed coarse-grained ferrimagnetic LLB model and the atomistic code VAMPIRE. (a) Easy axis loop at a constant temperature of (a) 100 K and (b) 500 K. Hysteresis loop with the applied field tilted 45° against the z direction at a constant temperature of (c) 100 K and (d) 500 K.

$\Lambda(T)$. Figure 4 reveals the second problem of the atomistic data. At low temperatures, far away from the Curie point, mean field values and atomistic data significantly differ. For example, at 300 K the discrepancy is about one order of magnitude. Ultimately, the high values of Λ lead to a considerably slower relaxation of the magnetization of the sublattices compared to atomistic simulations, especially at intermediate temperatures.

The reason why this approach of extracting Λ from atomistic data does not work for ferrimagnets goes beyond the scope of this work and should be the subject of further research. In fact, at temperatures near T_C the leading term of Λ is the quotient of the longitudinal susceptibilities. Since, both $\tilde{\chi}_B^{\parallel}$ and $\tilde{\chi}_A^{\parallel}$ have the same finite-size effects, it makes sense that these effects cancel out if the quotient of the susceptibilities is evaluated. At low temperatures the mean-field expression should be correct anyway. Therefore, it is justified that $\Lambda_{AA}(T)$ and $\Lambda_{BB}(T)$ are calculated with the corresponding mean-field expression.

III. RESULTS

In order to confirm the validity of the proposed coarse-grained model, numerical tests for the presented $Gd_{30}(FeCo)_{70}$ system (see Table I) are performed in the following. First, the dynamics of single magnetization trajectories under the influence of heat and magnetic field are compared with corresponding trajectories computed with the atomistic code VAMPIRE. In Fig. 5(a) a constant temperature of 500 K and a constant magnetic field of -0.8 T are applied to the ferrimagnet. Field and easy axis of the grain (along the z direction) enclose an angle of 6°. 500 K is well above the compensation point and the ferrimagnet is FeCo dominated. The simulations are started with an initial magnetization of the FeCo sublattice in the positive z direction and the Gd sublattice magnetization pointing in the negative z direction. Unless otherwise stated, this initial configuration is used for all subsequent simulations. Figure 5(a) illustrates that the temporal evolution of m_z of both sublattices obtained by the proposed coarse-grained model agrees very well with the resulting VAMPIRE trajectories.

In a second test we investigate the magnetization dynamics under a heat pulse, without an external field. A Gaussian shaped heat pulse is used,

$$T(t) = T_{\text{min}} + (T_{\text{max}} - T_{\text{min}}) e^{(t-t_0)^2/\tau^2}, \tag{33}$$

with $T_{\text{min}} = 300$ K, $T_{\text{max}} = 600$ K, $t_0 = 0.3$ ns, and $\tau = 0.1$ ns. The temperature pulse starts slightly below the compensation point and heats the ferrimagnet near T_C, before the system cools down again. Temperature pulse and m_z of both sublattices are shown in Fig. 5(b). The results of our coarse-grained model and VAMPIRE again agree perfectly.

In a next step hysteresis loops at constant temperatures are compared. We analyze easy axis loops and loops with a field angle of 45° with respect to the easy axis of the ferrimagnet. The loops start with a saturating field with a magnitude of 3 T, which is decreased with a rate of 1 T per nanosecond until -3 T is reached. After that the field is again increased to 3 T. The choice of the fast field rate results from the high computational effort of atomistic simulations. All loops are calculated at two different temperatures, 100 and 500 K. Figure 6 displays the calculated hysteresis loops of the total normalized magnetization of the ferrimagnet for the four

cases. Again, the coarse-grained ferrimagnetic LLB model is in good agreement with atomistic VAMPIRE simulations.

In a last validation step switching probabilities of $Gd_{30}(FeCo)_{70}$ under the influence of various Gaussian heat pulses and a constant external field are analyzed. Again, a field with constant magnitude and a field angle of 6° with the z direction tries to align the total magnetization of the ferrimagnet along the negative z direction. Additionally, a heat pulse, according to Eq. (33), with $T_{\min} = 300$ K and various $T_{\max}$ is applied to the ferrimagnetic particle. For each $T_{\max}$, from 300 to 900 K with $\Delta T_{\max} = 20$ K, 128 trajectories are computed. The switching probability then corresponds to the proportion of successfully aligned particles compared to the total number of all started simulations. Two different field magnitudes and pulse durations are compared in Fig. 7. In the case of a long pulse duration of $\tau = 100$ ps, which is for example typical in heat-assisted magnetic recording, the comparison of the switching probabilities obtained by the coarse-grained ferrimagnetic LLB model and VAMPIRE simulations in Figs. 7(a) and 7(b) confirms the desired perfect agreement of the ferrimagnetic LLB model. To check the influence of the temperature dependence of the perpendicular susceptibility in the ferrimagnetic LLB model, which was introduced in Sec. II C, the probabilities are recomputed with the same setup, with the only difference that a constant anisotropy field, $H_{\text{ani,A}} = 2d_{\text{A}}/\mu_{\text{A}}$, is used. The resulting probabilities, as illustrated in Fig. 7(a), show a completely different behavior. This fact strengthens the conclusion that it is important to consider the temperature dependence of the anisotropy field in the coarse-grained ferrimagnetic LLB model.

For shorter heat pulses of $\tau = 10$ ps the agreement of ferrimagnetic LLB model and atomistic simulations is still good, but at temperatures well above the Curie point the probabilities slightly differ. The ferrimagnetic LLB model tends to underestimate the switching probabilities compared to the VAMPIRE simulations. However, the difference is still within the statistical variation range of the switching probabilities, as can be seen in Fig. 7(c) at $T_{\max} = 840$ K.

At this point, we would like to return briefly to the discussion of Sec. II C about how to model $\Lambda(T)$. We additionally computed the switching probabilities of Fig. 7 with $\Lambda(T)$ extracted directly from atomistic data (see Fig. 4). The agreement with switching probabilities obtained from VAMPIRE simulations for heat pulses with a pulse duration of $\tau = 100$ ps is again remarkably good. For shorter pulses with $\tau = 10$ ps the deviation from atomistic results becomes significant, in contrast to the ferrimagnetic LLB model with $\Lambda(T)$ calculated with the mean-field model [see Fig. 7(c)]. The shorter longitudinal relaxation times, originating form the smaller values of the mean field $\Lambda(T)$, only seem to play an important role for very fast processes. Nevertheless, the reason for the discrepancy between atomistic and mean field $\Lambda(T)$ is not obvious and should be the subject of further research.

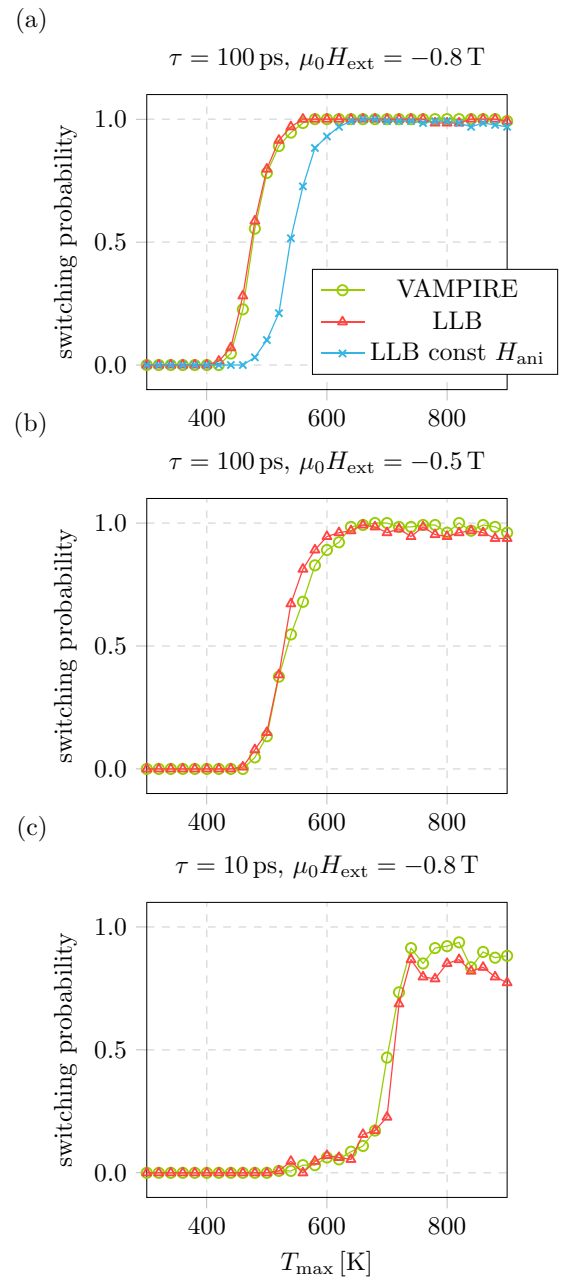

FIG. 7. Switching probabilities of a $Gd_{30}(FeCo)_{70}$ particle computed from 128 switching trajectories at each $T_{\max}$. In each simulation a constant field and a Gaussian shaped heat pulse according to Eq. (33) with $T_{\min} = 300$ K are applied. Two different field magnitudes $\mu_0 H_{\text{ext}} = -0.5$ T and $\mu_0 H_{\text{ext}} = -0.8$ T as well as two different pulse durations $\tau = 100$ ps and $\tau = 10$ ps are compared. Atomistic simulations with VAMPIRE are compared with the proposed coarse-grained LLB model. Additionally in (a) the LLB model with a constant anisotropy field [Eq. (6)] is illustrated.

All-optical switching

The ultimate goal is to describe all-optical switching (AOS) of finite magnetic particles with the ferrimagnetic LLB equation, which allows us to compute switching probabilities with little computational effort. As a consequence AOS could ultimately be investigated as a potential recording technique. Although the magnetization trajectories are short, the effort to investigate whole phase spaces of recording parameters for atomistic simulations is tremendous. A simple two-spin model would furthermore show the underlying physical effects of

TABLE II. Material parameters of $Gd_{25}(FeCo)_{75}$ (taken from Ref. [16]). d is the anisotropy energy per atom, μ is the magnetic moment in units of Bohr magnetons, x is the FeCo concentration, $J_{\kappa\text{-}\kappa}$ denotes the exchange energy per atom link between equal atoms, $J_{\kappa\text{-}\nu}$ denotes the exchange energy per atom link between different atoms, and λ is the damping constant.

	FeCo	Gd
d (J)	8.07251×10^{-24}	8.07251×10^{-24}
μ (μ_{Bohr})	1.92	7.63
x (%)	75	25
$J_{\kappa-\kappa}$ (J)	2.835×10^{-21}	1.26×10^{-21}
$J_{\kappa-\nu}$ (J)	-1.09×10^{-21}	
λ	0.05	0.05

AOS more clearly. For better comparability with Ref. [16], we use $Gd_{25}(FeCo)_{75}$ particles according to Table II in the following. The geometry is the same as in Table I and the material functions are illustrated in Fig. 8. Note that due to the smaller damping of $Gd_{25}(FeCo)_{75}$ a smaller time step of 10^{-16} s is used in the atomistic simulations.

We apply a short heat pulse with a duration of 50 fs, a starting temperature of 300 K, and a maximum temperature of 1193 K to the particle. The electronic temperature pulse is calculated with the two-temperature model [48]. For reasons of efficiency, we do not repeat the two-temperature model here, but rather directly illustrate the applied temperature pulse in Fig. 9. The initial direction of the FeCo magnetization is set to the positive z direction and that of the Co magnetization in the negative z direction. At first glance the magnetization dynamics are in good agreement as shown in Fig. 9(a). During the equilibration phase ($t < 10$ ps) the dynamics of the atomistic simulations and the LLB simulations match perfectly. In both cases the heat pulse switches the sublattices and after the heat pulse the reestablishment of the magnetization also agrees well. Figure 9(b), illustrating the angle ϕ between the FeCo and Gd magnetizations (average magnetizations in the case of atomistic simulations), points out that the simulation with the stochastic ferrimagnetic LLB equation shows a ferromagneticlike state of the sublattices, which was found to be the key for AOS in GdFeCo [16,23]. This is an important result because studies with the deterministic ferrimagnetic LLB equation had to artificially introduce an angle between the sublattices to show AOS [41,42]. And even then, no ferromagneticlike state during AOS was observed. With the derived stochastic version of the ferrimagnetic LLB equation switching with a ferromagneticlike state comes out in a natural way.

Despite these promising results, no perfect agreement of atomistic and LLB model could be obtained, because the switching probability of 128 AOS trial trajectories, equivalent to that shown in Fig. 9, is just 11% for LLB simulations. In contrast, the probability is 86% in the case of VAMPIRE simulations. That the atomistic simulations do not reach $p = 1$ may be attributed to the fact that we only simulated a small particle with less than 60 000 spins. In other works [16,23], which show deterministic AOS, about ten times larger particles were considered. Nevertheless, the switching probability is clearly above 50% and thus a purely thermal effect of a vanishing net

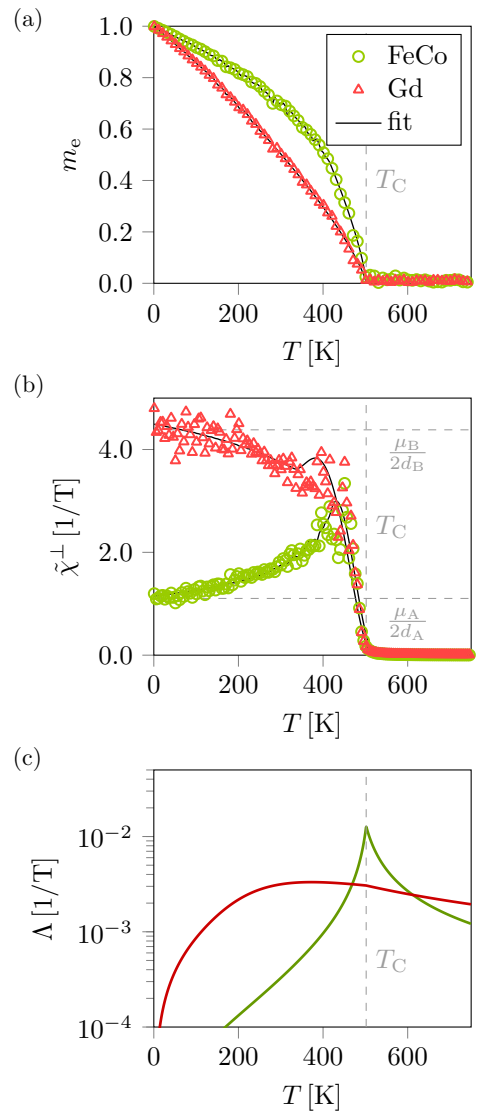

FIG. 8. Temperature-dependent material functions for $Gd_{25}(FeCo)_{75}$ (parameters are given in Table II). (a) Zero-field equilibrium magnetization m_e, (b) perpendicular susceptibility $\tilde{\chi}^{\perp}$, (c) Λ computed with the mean field expression of Eq. (15) vs temperature. The black solid lines show fits of the given atomistic data, representing an infinite system.

magnetization of the sublattices and the subsequent remagnetization in a random direction can be discarded as the cause. A possible reason for the different switching probabilities of the coarse-grained LLB model and the atomistic model can be found in Fig. 9(c). The figure displays the actual switching process of Fig. 9(a) in more detail. It can be seen that the reversal of both sublattices is significantly faster in case of the LLB model. The FeCo sublattice still reverses faster than the Gd sublattice, but the difference in demagnetization rates decreases. The effect of a faster longitudinal relaxation of the Gd sublattice was already observed for the deterministic ferrimagnetic LLB equation in Ref. [41]. The authors argued with large deviations from equilibrium for sudden and high temperature steps. Possibly, higher-order corrections are indeed needed in the ferrimagnetic LLB, as already suggested in

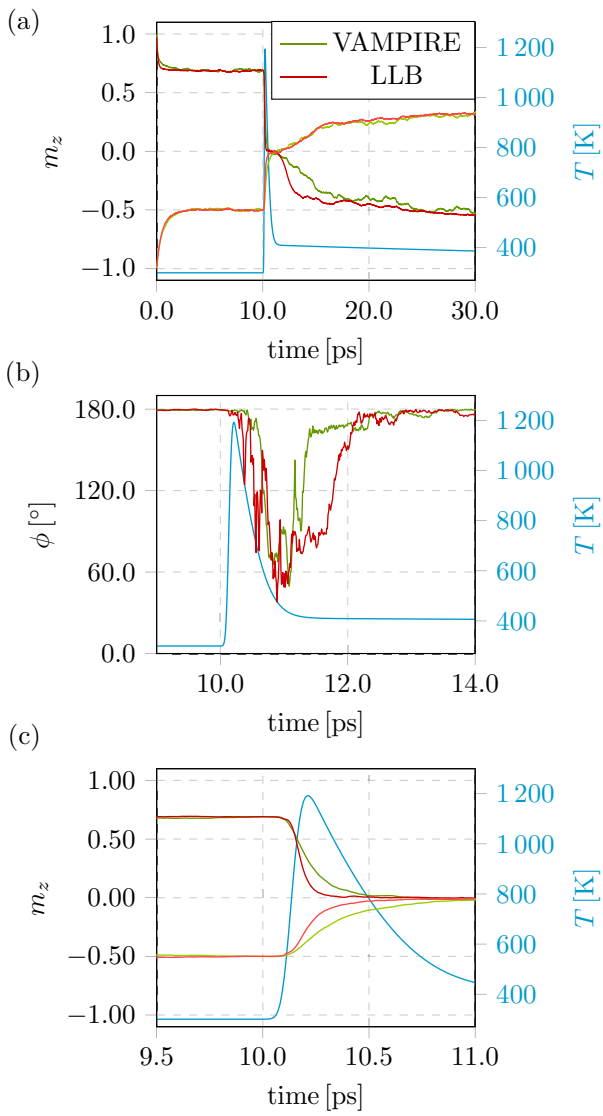

FIG. 9. Temporal evolution (a) of the z component of the normalized sublattice magnetizations and (b) of the angle between the sublattices of $Gd_{25}(FeCo)_{75}$ (see Table II). The illustrated heat pulse with a duration of 50 fs is applied to the particle. The trajectories are computed with the derived coarse-grained LLB model and the atomistic code VAMPIRE. (c) Zoom of the switching process in (a).

Ref. [41]. For synthetic ferrimagnets it was shown in Ref. [49] that the demagnetization time is mainly determined by the atomic spin moment and the damping of the material. Thus, a correction of the damping term could be a good starting point. In any case, the solution of this problem requires further research.

IV. CONCLUSION

In this work we developed a coarse-grained model of disordered ferrimagnets based on the ferrimagnetic Landau-Lifshitz-Bloch equation [40]. In a first step, stochastic fields were incorporated into the ferrimagnetic LLB equation in order to account for thermal fluctuations of individual system trajectories. In a second step, an expression for the perpendicular susceptibilities of finite-sized ferrimagnets was derived from thermodynamics. As with the LLB equation of ferromagnets, modeling the temperature-dependent susceptibilities and the zero-field equilibrium magnetization is the key to accurately describing the magnetization dynamics of ferrimagnets with high computational efficiency. We have shown that the presented coarse-grained model agrees well with atomistic simulations, in which the stochastic Landau-Lifshitz-Gilbert equation is solved for each atom of a particle. The agreement was proven for simulations of a small GdFeCo ferrimagnetic particle with 70% FeCo and 30% Gd with a diameter of 5 nm and a length of 10 nm subject to various external applied fields and heat pulses with a duration of 10 ps and longer.

In a last step we investigated all-optical switching (AOS) of a $Gd_{25}(FeCo)_{75}$ particle with the same size by applying a 50-fs heat pulse with a maximum temperature of 1193 K to the particle. We could observe switching without having to make any further assumptions, such as a tilting of the magnetizations of the sublattices. Additionally, a ferromagneticlike state appeared. This state was indicated as the key for AOS in GdFeCo and so far could not be reproduced with a ferrimagnetic LLB model.

However, the switching probability under the influence of the ultrashort heat pulse was significantly lower for the LLB model than for an atomistic model. Although the comparison of the magnetization dynamics of the two models shows good agreement at first glance, a closer look reveals a significantly faster longitudinal relaxation of the LLB model when applying the ultrafast heat pulse. Especially this faster relaxation affects the Gd sublattice, which reduces the difference of the relaxation constants of the two sublattices, which is unfavorable for AOS. This observation supports the suspicion that the model fails too far away from equilibrium and therefore higher-order corrections may be necessary. Since the switching probability was even lower than 50% we do not have any insights into deterministic AOS. The fact that the agreement with atomistic simulations for longer heat pulses is very good raises the question whether the two-spin LLB model is capable of describing AOS at all. Here, further research is required.

Nonetheless, we are convinced that this work provides an important step towards a better understanding of AOS. In the case of longer heat pulses of several picoseconds and more, the proposed model of finite-sized disordered ferrimagnets shows already good agreement with a much more time consuming atomistic model. The fact that ferrimagnetic materials are becoming increasingly interesting for applications, especially for any kind of magneto-optical recording or MRAM, further shows the importance of this work.

ACKNOWLEDGMENTS

The authors would like to thank the Vienna Science and Technology Fund (WWTF) under Grant No. MA14-044, the Advanced Storage Technology Consortium (ASTC), and the Austrian Science Fund (FWF) under Grant No. I2214-N20 for financial support. The computational results presented have been achieved using the Vienna Scientific Cluster (VSC).

APPENDIX: DIFFUSION CONSTANTS OF THE STOCHASTIC FERRIMAGNETIC LLB EQUATION

As discussed in Sec. II A thermal fluctuations can be introduced to the LLB equation via thermal fields, with components consisting of white-noise random numbers with zero mean and a variance of

$$\left\langle \xi^{\eta}_{\kappa,i}(t,\boldsymbol{r})\xi^{\eta}_{\kappa,j}(t',\boldsymbol{r}')\right\rangle = 2D^{\eta}_{\kappa}\delta_{ij}\delta(\boldsymbol{r}-\boldsymbol{r}')\delta(t-t'). \tag{A1}$$

The main objective is now to determine the coefficients D^{η}_{ν}, which are a measure for the magnitude of thermal fluctuations. The starting point for the derivation is the most general form of the LLB equation, which can be written as a multivariate Langevin equation:

$$\frac{dm_i}{dt} = a_i(\boldsymbol{m},t) + \sum_{k\eta} b^{\eta}_{ik}(\boldsymbol{m},t)\xi^{\eta}_{k}(t). \tag{A2}$$

If the vector $a_i(\boldsymbol{m},t)$ and the tensor $b_{ik}(\boldsymbol{m},t)$ are known the corresponding Fokker-Planck (FP) equation can be directly constructed per

$$\frac{\partial\rho}{\partial t} = -\sum_i \frac{\partial}{\partial m_i}\Bigg[\Bigg(a_i - \sum_{\eta} D^{\eta}\sum_k b^{\eta}_{ik}\sum_j \frac{\partial b^{\eta}_{jk}}{\partial m_j} - \sum_{\eta} D^{\eta}\sum_{jk} b^{\eta}_{ik}b^{\eta}_{jk}\frac{\partial}{\partial m_j}\Bigg)\rho\Bigg]. \tag{A3}$$

This equation describes the temporal evolution of the probability density $\rho(\boldsymbol{m},t)$ of finding a magnetic configuration with magnetization $\boldsymbol{m}$ at time t. In accordance with the ferromagnetic case we define $a_{\mathrm{A},i}(\boldsymbol{m},t)$ and $b_{\mathrm{A},ik}(\boldsymbol{m},t)$ for sublattice A as follows:

$$\begin{aligned} a_{\mathrm{A},i}(\boldsymbol{m}_{\mathrm{A}},t) &= -\gamma'_{\mathrm{A}}\mu_0(\boldsymbol{m}_{\mathrm{A}}\times\boldsymbol{H}_{\mathrm{eff}}) \\ &\quad - \frac{\alpha^{\perp}_{\mathrm{A}}\gamma'_{\mathrm{A}}\mu_0}{m^2_{\mathrm{A}}}[\boldsymbol{m}_{\mathrm{A}}\times(\boldsymbol{m}_{\mathrm{A}}\times\boldsymbol{H}_{\mathrm{eff}})] \\ &\quad + \frac{\alpha^{\parallel}_{\mathrm{A}}\gamma'_{\mathrm{A}}\mu_0}{m^2_{\mathrm{A}}}\boldsymbol{m}_{\mathrm{A}}(\boldsymbol{m}_{\mathrm{A}}\cdot\boldsymbol{H}_{\mathrm{eff}}), \end{aligned} \tag{A4}$$

and

$$\begin{aligned} b^{\parallel}_{\mathrm{A},ik}(\boldsymbol{m}_{\mathrm{A}},t) &= \delta_{ik}, \\ b^{\perp}_{\mathrm{A},ik}(\boldsymbol{m}_{\mathrm{A}},t) &= \alpha^{\perp}_{\mathrm{A}}\gamma'_{\mathrm{A}}\mu_0\left(\delta_{ik} - \frac{m_{\mathrm{A},i}m_{\mathrm{A},k}}{m^2_{\mathrm{A}}}\right). \end{aligned} \tag{A5}$$

Inserting Eqs. (A4) and (A5) into Eq. (A3) yields the FP equation for the sublattice,

$$\begin{aligned} \frac{\partial\rho_{\mathrm{A}}}{\partial t} &= -\frac{\partial}{\partial\boldsymbol{m}_{\mathrm{A}}}\cdot\Bigg\{\Bigg[-\gamma'_{\mathrm{A}}\mu_0(\boldsymbol{m}_{\mathrm{A}}\times\boldsymbol{H}_{\mathrm{eff}}) \\ &\quad - \frac{\alpha^{\perp}_{\mathrm{A}}\gamma'_{\mathrm{A}}\mu_0}{m^2_{\mathrm{A}}}\boldsymbol{m}_{\mathrm{A}}\times(\boldsymbol{m}_{\mathrm{A}}\times\boldsymbol{H}_{\mathrm{eff}}) \\ &\quad + \frac{\alpha^{\parallel}_{\mathrm{A}}\gamma'_{\mathrm{A}}\mu_0}{m^2_{\mathrm{A}}}\boldsymbol{m}_{\mathrm{A}}(\boldsymbol{m}_{\mathrm{A}}\cdot\boldsymbol{H}_{\mathrm{eff}}) + \frac{D^{\perp}_{\mathrm{A}}(\alpha^{\perp}_{\mathrm{A}}\gamma'_{\mathrm{A}}\mu_0)^2}{m^2_{\mathrm{A}}}\boldsymbol{m}_{\mathrm{A}} \\ &\quad \times\left(\boldsymbol{m}_{\mathrm{A}}\times\frac{\partial}{\partial\boldsymbol{m}_{\mathrm{A}}}\right) - D^{\parallel}_{\mathrm{A}}\frac{\partial}{\partial\boldsymbol{m}_{\mathrm{A}}}\Bigg]\rho_{\mathrm{A}}\Bigg\}. \end{aligned} \tag{A6}$$

To compute the diffusion constants we assume that in equilibrium the probability density of each sublattice magnetization follows a Boltzmann distribution per

$$\rho_{\mathrm{A}} = \rho_{\mathrm{A},0}\exp[-E(\boldsymbol{m}_{\mathrm{A}})/k_{\mathrm{B}}T], \tag{A7}$$

$$\frac{\partial\rho_{\mathrm{A}}}{\partial\boldsymbol{m}_{\mathrm{A}}} = \rho_{\mathrm{A}}\frac{\mu_0 M_{\mathrm{A},0}V}{k_{\mathrm{B}}T}\boldsymbol{H}_{\mathrm{eff}} = \rho_{\mathrm{A}}\frac{\mu_0 n_{\mathrm{at}}x_{\mathrm{A}}\mu_{\mathrm{A}}V}{l^3_{\mathrm{at}}k_{\mathrm{B}}T}\boldsymbol{H}_{\mathrm{eff}}. \tag{A8}$$

This equation holds for a discrete system with discretization volume V. In the last term of Eq. (A8) we identified the total magnetic moment of sublattice A with atomistic quantities. Here, x_{A} is the concentration of atoms A, l_{at} is the lattice constant, and n_{at} is the number of atoms per unit cell. Using the expression of Eq. (A8) in the FP equation and demanding that $\partial\rho_{\mathrm{A}}/\partial t = 0$ is valid in equilibrium, the diffusion constants of sublattice A can be computed as

$$D^{\perp}_{\mathrm{A}} = \frac{(\alpha^{\perp}_{\mathrm{A}} - \alpha^{\parallel}_{\mathrm{A}})l^3_{\mathrm{at}}k_{\mathrm{B}}T}{(\alpha^{\perp}_{\mathrm{A}})^2\gamma'_{\mathrm{A}}\mu^2_0 n_{\mathrm{at}}x_{\mathrm{A}}\mu_{\mathrm{A}}V}, \tag{A9}$$

$$D^{\parallel}_{\mathrm{A}} = \frac{\alpha^{\parallel}_{\mathrm{A}}\gamma'_{\mathrm{A}}l^3_{\mathrm{at}}k_{\mathrm{B}}T}{n_{\mathrm{at}}x_{\mathrm{A}}\mu_{\mathrm{A}}V}. \tag{A10}$$

Finally, the corresponding stochastic LLB equation for ferrimagnets can be obtained by using Eqs. (A4) and (A5) together with Eqs. (A9), (A10), and (A1) in the Langevin equation [Eq. (A2)] per

$$\begin{aligned} \frac{\partial\boldsymbol{m}_{\mathrm{A}}}{\partial t} &= -\mu_0\gamma'_{\mathrm{A}}(\boldsymbol{m}_{\mathrm{A}}\times\boldsymbol{H}_{\mathrm{eff,A}}) \\ &\quad + \frac{\mu_0\gamma'_{\mathrm{A}}\alpha^{\parallel}_{\mathrm{A}}}{m^2_{\mathrm{A}}}(\boldsymbol{m}_{\mathrm{A}}\cdot\boldsymbol{H}_{\mathrm{eff,A}})\boldsymbol{m}_{\mathrm{A}} + \boldsymbol{\xi}^{\parallel}_{A} \\ &\quad - \frac{\mu_0\gamma'_{\mathrm{A}}\alpha^{\perp}_{\mathrm{A}}}{m^2_{\mathrm{A}}}\{\boldsymbol{m}_{\mathrm{A}}\times[\boldsymbol{m}_{\mathrm{A}}\times(\boldsymbol{H}_{\mathrm{eff,A}} + \boldsymbol{\xi}^{\perp}_{A})]\}. \end{aligned} \tag{A11}$$

[1] L. Mayer, J. Appl. Phys. **29**, 1003 (1958).

[2] C. Mee and G. Fan, IEEE Trans. Magn. **3**, 72 (1967).

[3] G. W. Lewicki and J. E. Guisinger, US Patent No. US3626114 (10 March 1969).

[4] H. Kobayashi, M. Tanaka, H. Machida, T. Yano, and U. M. Hwang, JP Patent No. JPS57113402 (5 January 1984).

[5] R. Rottmayer, S. Batra, D. Buechel, W. Challener, J. Hohlfeld, Y. Kubota, L. Li, B. Lu, C. Mihalcea, K. Mountfield, K. Pelhos, C. Peng, T. Rausch, M. A. Seigler, D. Weller, and X. Yang, IEEE Trans. Magn. **42**, 2417 (2006).

[6] D. A. Garanin, Phys. Rev. B **55**, 3050 (1997).

[7] N. Kazantseva, D. Hinzke, U. Nowak, R. W. Chantrell, U. Atxitia, and O. Chubykalo-Fesenko, Phys. Rev. B **77**, 184428 (2008).

[8] R. F. L. Evans, D. Hinzke, U. Atxitia, U. Nowak, R. W. Chantrell, and O. Chubykalo-Fesenko, Phys. Rev. B **85**, 014433 (2012).

[9] C. Vogler, C. Abert, F. Bruckner, and D. Suess, Phys. Rev. B **90**, 214431 (2014).

[10] J.-G. Zhu and H. Li, IEEE Trans. Magn. **49**, 765 (2013).

[11] C. Vogler, C. Abert, F. Bruckner, D. Suess, and D. Praetorius, Appl. Phys. Lett. **108**, 102406 (2016).

[12] J.-G. Zhu and H. Li, IEEE Trans. Magn. **53**, 1 (2017).

[13] C. Vogler, C. Abert, F. Bruckner, and D. Suess, Appl. Phys. Lett. **110**, 182406 (2017).

[14] C. Vogler, C. Abert, F. Bruckner, and D. Suess, Phys. Rev. Appl. **8**, 054021 (2017).

[15] C. D. Stanciu, F. Hansteen, A. V. Kimel, A. Kirilyuk, A. Tsukamoto, A. Itoh, and T. Rasing, Phys. Rev. Lett. **99**, 047601 (2007).

[16] I. Radu, K. Vahaplar, C. Stamm, T. Kachel, N. Pontius, H. A. Dürr, T. A. Ostler, J. Barker, R. F. L. Evans, R. W. Chantrell, A. Tsukamoto, A. Itoh, A. Kirilyuk, T. Rasing, and A. V. Kimel, Nature **472**, 205 (2011).

[17] S. Alebrand, A. Hassdenteufel, D. Steil, M. Cinchetti, and M. Aeschlimann, Phys. Rev. B **85**, 092401 (2012).

[18] A. R. Khorsand, M. Savoini, A. Kirilyuk, A. V. Kimel, A. Tsukamoto, A. Itoh, and T. Rasing, Phys. Rev. Lett. **108**, 127205 (2012).

[19] K. Vahaplar, A. M. Kalashnikova, A. V. Kimel, S. Gerlach, D. Hinzke, U. Nowak, R. Chantrell, A. Tsukamoto, A. Itoh, A. Kirilyuk, and T. Rasing, Phys. Rev. B **85**, 104402 (2012).

[20] J. Barker, U. Atxitia, T. A. Ostler, O. Hovorka, O. Chubykalo-Fesenko, and R. W. Chantrell, Sci. Rep. **3**, 3262 (2013).

[21] A. Hassdenteufel, B. Hebler, C. Schubert, A. Liebig, M. Teich, M. Helm, M. Aeschlimann, M. Albrecht, and R. Bratschitsch, Adv. Mater. **25**, 3122 (2013).

[22] O. J. Suarez, P. Nieves, D. Laroze, D. Altbir, and O. Chubykalo-Fesenko, Phys. Rev. B **92**, 144425 (2015).

[23] T. A. Ostler, J. Barker, R. F. L. Evans, R. W. Chantrell, U. Atxitia, O. Chubykalo-Fesenko, S. E. Moussaoui, L. L. Guyader, E. Mengotti, L. J. Heyderman, F. Nolting, A. Tsukamoto, A. Itoh, D. Afanasiev, B. A. Ivanov, A. M. Kalashnikova, K. Vahaplar, J. Mentink, A. Kirilyuk, T. Rasing, and A. V. Kimel, Nat. Commun. **3**, 666 (2012).

[24] A. R. Khorsand, M. Savoini, A. Kirilyuk, A. V. Kimel, A. Tsukamoto, A. Itoh, and T. Rasing, Phys. Rev. Lett. **110**, 107205 (2013).

[25] S. Alebrand, M. Gottwald, M. Hehn, D. Steil, M. Cinchetti, D. Lacour, E. E. Fullerton, M. Aeschlimann, and S. Mangin, Appl. Phys. Lett. **101**, 162408 (2012).

[26] S. Alebrand, U. Bierbrauer, M. Hehn, M. Gottwald, O. Schmitt, D. Steil, E. E. Fullerton, S. Mangin, M. Cinchetti, and M. Aeschlimann, Phys. Rev. B **89**, 144404 (2014).

[27] M. S. El Hadri, P. Pirro, C.-H. Lambert, S. Petit-Watelot, Y. Quessab, M. Hehn, F. Montaigne, G. Malinowski, and S. Mangin, Phys. Rev. B **94**, 064412 (2016).

[28] R. Moreno, T. A. Ostler, R. W. Chantrell, and O. Chubykalo-Fesenko, Phys. Rev. B **96**, 014409 (2017).

[29] T.-M. Liu, T. Wang, A. H. Reid, M. Savoini, X. Wu, B. Koene, P. Granitzka, C. E. Graves, D. J. Higley, Z. Chen, G. Razinskas, M. Hantschmann, A. Scherz, J. Stöhr, A. Tsukamoto, B. Hecht, A. V. Kimel, A. Kirilyuk, T. Rasing, and H. A. Dürr, Nano Lett. **15**, 6862 (2015).

[30] C. Schubert, A. Hassdenteufel, P. Matthes, J. Schmidt, M. Helm, R. Bratschitsch, and M. Albrecht, Appl. Phys. Lett. **104**, 082406 (2014).

[31] S. Mangin, M. Gottwald, C.-H. Lambert, D. Steil, V. Uhlíř, L. Pang, M. Hehn, S. Alebrand, M. Cinchetti, G. Malinowski, Y. Fainman, M. Aeschlimann, and E. E. Fullerton, Nat. Mater. **13**, 286 (2014).

[32] Z. Zhao, M. Jamali, A. K. Smith, and J.-P. Wang, Appl. Phys. Lett. **106**, 132404 (2015).

[33] J. Finley and L. Liu, Phys. Rev. Appl. **6**, 054001 (2016).

[34] K. Ueda, M. Mann, C.-F. Pai, A.-J. Tan, and G. S. D. Beach, Appl. Phys. Lett. **109**, 232403 (2016).

[35] N. Roschewsky, T. Matsumura, S. Cheema, F. Hellman, T. Kato, S. Iwata, and S. Salahuddin, Appl. Phys. Lett. **109**, 112403 (2016).

[36] W. Seung Ham, S. Kim, D.-H. Kim, K.-J. Kim, T. Okuno, H. Yoshikawa, A. Tsukamoto, T. Moriyama, and T. Ono, Appl. Phys. Lett. **110**, 242405 (2017).

[37] R. Mishra, J. Yu, X. Qiu, M. Motapothula, T. Venkatesan, and H. Yang, Phys. Rev. Lett. **118**, 167201 (2017).

[38] N. Roschewsky, C.-H. Lambert, and S. Salahuddin, Phys. Rev. B **96**, 064406 (2017).

[39] B. Dai, Y. Guo, J. Zhu, T. Kato, S. Iwata, S. Tsunashima, L. Yang, and J. Han, J. Phys. D: Appl. Phys. **50**, 135005 (2017).

[40] U. Atxitia, P. Nieves, and O. Chubykalo-Fesenko, Phys. Rev. B **86**, 104414 (2012).

[41] P. Nieves, U. Atxitia, R. W. Chantrell, and O. Chubykalo-Fesenko, Low Temp. Phys. **41**, 739 (2015).

[42] U. Atxitia, T. Ostler, J. Barker, R. F. L. Evans, R. W. Chantrell, and O. Chubykalo-Fesenko, Phys. Rev. B **87**, 224417 (2013).

[43] U. Atxitia, J. Barker, R. W. Chantrell, and O. Chubykalo-Fesenko, Phys. Rev. B **89**, 224421 (2014).

[44] D. Hinzke, U. Atxitia, K. Carva, P. Nieves, O. Chubykalo-Fesenko, P. M. Oppeneer, and U. Nowak, Phys. Rev. B **92**, 054412 (2015).

[45] U. Atxitia, D. Hinzke, and U. Nowak, J. Phys. D: Appl. Phys. **50**, 033003 (2017).

[46] C. Vogler, C. Abert, F. Bruckner, D. Suess, and D. Praetorius, J. Appl. Phys. **120**, 223903 (2016).

[47] R. F. L. Evans, W. J. Fan, P. Chureemart, T. A. Ostler, M. O. A. Ellis, and R. W. Chantrell, J. Phys.: Condens. Matter **26**, 103202 (2014).

[48] J. Chen, D. Tzou, and J. Beraun, Int. J. Heat Mass Transfer **49**, 307 (2006).

[49] R. F. L. Evans, T. A. Ostler, R. W. Chantrell, I. Radu, and T. Rasing, Appl. Phys. Lett. **104**, 082410 (2014).